Effects of Wave Streaming and Wave Variations on Nearshore Wave-Driven Circulation

PENG WANG,[a] JAMES C. MCWILLIAMS,[a] YUSUKE UCHIYAMA,[b] MICKAËL D. CHEKROUN,[a] AND DALING LI YI[c]

[a] *Department of Atmospheric and Oceanic Sciences, University of California, Los Angeles, Los Angeles, California;* [b] *Department of Civil Engineering, Kobe University, Kobe, Japan;* [c] *International Pacific Research Center, School of Ocean and Earth Science and Technology, University of Hawai'i at Mānoa, Honolulu, Hawaii*

(Manuscript received 3 December 2019, in final form 30 June 2020)

ABSTRACT: Wave streaming is a near-bottom mean current induced by the bottom drag on surface gravity waves. Wave variations include the variations in wave heights, periods, and directions. Here we use numerical simulations to study the effects of wave streaming and wave variations on the circulation that is driven by incident surface waves. Wave streaming induces an inner-shelf Lagrangian overturning circulation, which links the inner shelf with the surf zone. Wave variations cause alongshore-variable wave breaking that produces surf eddies; however, such eddies can be suppressed by wave streaming. Moreover, with passive tracers we show that wave streaming and wave variations together enhance the cross-shelf material transport.

KEYWORDS: Bottom currents; Coastal flows; Waves, oceanic; Lagrangian circulation/transport

1. Introduction

The nearshore region that includes a surf zone and an inner shelf is important to the marine ecosystem and human health (Ryan et al. 2005; Pineda et al. 2007; Kumar and Feddersen 2017a). The surf zone is where surface waves break due to shallow depths (Battjes 1988; MacMahan et al. 2006). Next to the surf zone seaward, the inner shelf is where the surface and bottom boundary layers overlap (Nittrouer and Wright 1994; Lentz 1995).

One of the critical processes to sustain the nearshore ecosystem is the cross-shelf material transport, such as the transport of nutrients, pollutants, and plankton (Shanks et al. 2015; Fujimura et al. 2018; Morgan et al. 2018). The cross-shelf material transport is controlled by many processes (Dalrymple et al. 2011; Lentz and Fewings 2012; Brink 2016; Castelle et al. 2016; Trowbridge and Lentz 2018). For example, rip currents and surf eddies dominate the material transport between the surf zone and inner shelf (Hally-Rosendahl et al. 2014; Suanda and Feddersen 2015; Spydell et al. 2019); particularly, bathymetric rip currents due to alongshore-variable bathymetry (e.g., rip channels) can trap materials within the persistent horizontal recirculations (MacMahan et al. 2010; Reniers et al. 2010; Brown et al. 2015). Besides, internal bores can carry materials within a water mass (e.g., heat, salt, and larvae) from the inner shelf to the surf zone (Pineda 1994; Sinnett et al. 2018).

Another process important to the cross-shelf material transport is the wave streaming. In shallow water, surface waves are subject to bottom drag, which induces a near-bottom current along the wave propagation. This current is referred to as wave bottom streaming (Longuet-Higgins 1953). The onset of wave bottom streaming depends on the wavelength; long waves like swells are able to feel bottom drag in deeper water, and subsequently the wave bottom streaming commences there. Nonetheless, the wave bottom streaming may be reduced under nonlinear waves (Trowbridge and Madsen 1984; Davies and Villaret 1999; van der A et al. 2011; Kranenburg et al. 2012; Henriquez et al. 2014). In addition, the viscous stress within the wave surface boundary layer can cause wave surface streaming (Longuet-Higgins 1953), which might be important to the upper ocean transport (Madsen 1978; Weber et al. 2006; Wang and Özgökmen 2018); however, it is negligible in this study, in agreement with Uchiyama et al. (2010). Thus, we focus on the wave bottom streaming only and for simplicity call it ''wave streaming.''

Wave streaming is important to the sediment transport and can shape the bed forms (Reniers et al. 2004a; Nielsen 2006; Ruessink et al. 2009; Reniers et al. 2013). Besides, wave streaming delivers plankton and larvae from the inner shelf to the surf zone, which is a crucial migration for some marine species (Pineda et al. 2007; Shanks et al. 2015; Fujimura et al. 2018; Morgan et al. 2018). Moreover, using observations in a water depth of 12 m, Lentz et al. (2008) measured an onshore current of $0.5\,\mathrm{cm\,s^{-1}}$ at 2 m above the bottom (cf. their Fig. 10a), and they claimed that this current may be related to tides; in addition to tides, however, other processes like the onshore wave streaming may also contribute to this current. Further, wave streaming decreases rapidly away from the bottom, and the deepest measurement in Lentz et al. (2008) is still far away from the bottom; thus, their measurements cannot adequately resolve the wave streaming profiles. Due to the importance and poor understanding of wave streaming, more field observations are needed, especially in the inner shelf.

In addition, realistic surface waves contain variations in wave heights, periods, and directions. These wave variations cause alongshore-variable wave breaking that generates surf eddies (Bowen 1969; Peregrine 1998; Clark et al. 2012). The surf-eddy generation mechanism due to wave variations can be as important as that due to shear instabilities of surf-zone alongshore currents (Long and Özkan-Haller 2009; Feddersen 2014). Further, wave variations inherently reside in wave

Corresponding author: Peng Wang, pwang@atmos.ucla.edu

DOI: 10.1175/JPO-D-19-0304.1

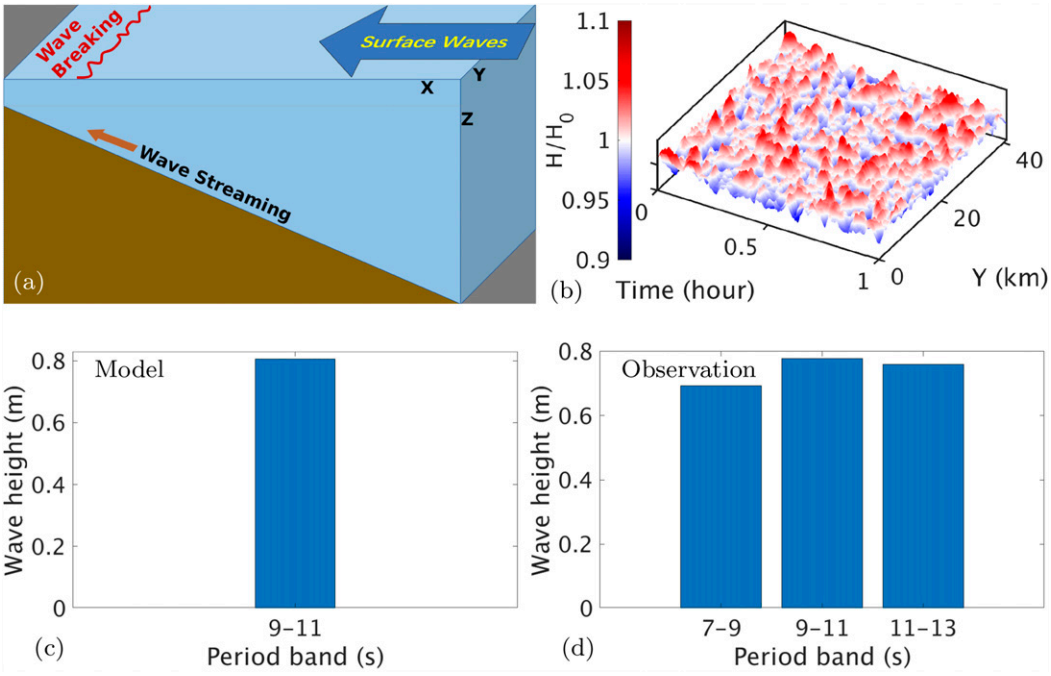

FIG. 1. (a) A schematic illustration of the numerical experiments. (b) A time series of stochastic wave heights at the offshore boundary, with a mean height of $H_0 = 0.8$ m. (c),(d) The wave heights averaged in each period band from the (c) stochastic waves and (d) realistic waves measured by a CDIP wave buoy (station 217 from 9 October 2019 to 9 November 2019).

groups, and surf eddies due to wave-group variations can develop spatial and temporal scales related to the wave groups (Reniers et al. 2004b; Long and Özkan-Haller 2009; MacMahan et al. 2010).

In the nearshore region, wave streaming and wave variations exist simultaneously. Then, how important are the wave streaming and wave variations to the nearshore wave-driven circulation? How do they together impact the cross-shelf material transport? Here we aim to answer these questions using numerical simulations. The structure of this study is as follows. The numerical model and experimental setup are described in section 2. The major results are presented in section 3, which are the mean flow, surf eddies, and the associated material transport. Moreover, sensitivity tests of the circulation are reported in section 4, and the study is concluded in section 5.

2. Methods

a. Numerical model

The experiments are simulated with a coupled wave–circulation model, which is the Regional Oceanic Modeling System (ROMS) fully coupled with a phase-averaged wave model (Uchiyama et al. 2010); thus, both wave effects on currents (WEC) and current effects on waves (CEW) are taken into account. The WEC contain two parts, i.e., conservative and nonconservative. The conservative WEC are based on the wave-averaged theory by McWilliams et al. (2004), including the Stokes vortex force (Craik and Leibovich 1976), Stokes–Coriolis force (Hasselmann 1970), and pressure adjustments. The nonconservative WEC are parameterized in terms of the wave dissipation, such as the wave breaking, wave streaming, and wave-enhanced current bottom drag. The model is briefly described in appendix A.

Our model has been validated against the nearshore measurements; it is able to reproduce the measured current profiles and wave characteristics (Uchiyama et al. 2010; Marchesiello et al. 2015). In our experiments, the parameters of wave forces are chosen based on those model validations, so that the simulated wave-driven circulation is reasonable compared to reality.

b. Experimental setup

The bathymetry is an alongshore-uniform shelf with a slope of 0.005 (Fig. 1a), which is a typically gentle slope for the inner shelf. The depth increases linearly from 0.3 to 205.1 m offshore. The horizontal lengths in the cross-shelf (X) and along-shelf (Y) directions are both equal to 40.96 km, with a horizontal resolution of 40 m. There are 12 vertical terrain-following layers that are denser near the surface and bottom to better resolve the boundary layers. Also, a comparison with 24

TABLE 1. Types of incident waves.

Incident waves	Uniform waves	Stochastic waves
Normal incidence (0°)	UN	SN
Oblique incidence (30°)	UO	SO

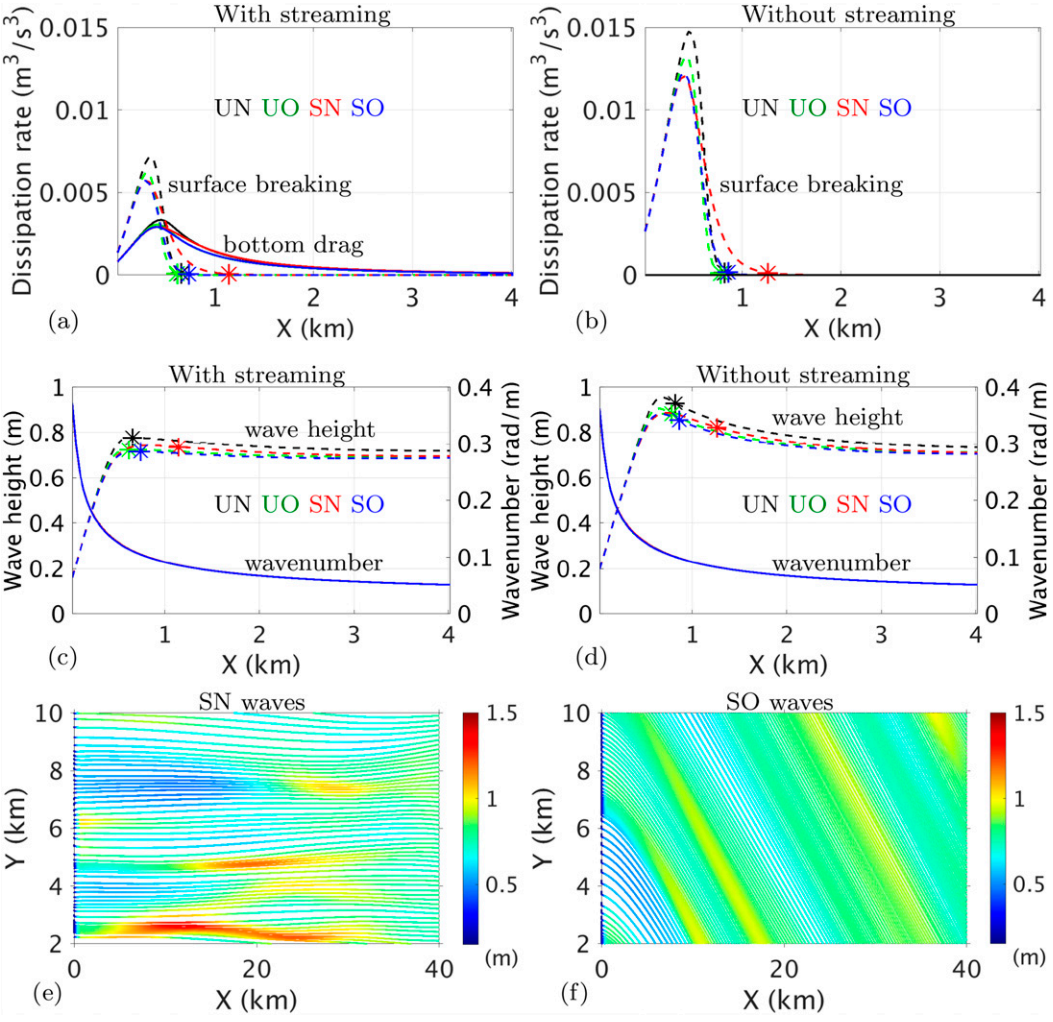

FIG. 2. (a),(b) Cross-shelf profiles of the mean wave dissipation by the bottom drag $\langle \overline{\varepsilon^f/\rho_0} \rangle$ [Eq. (A5); solid lines] and by the surface breaking $\langle \overline{\varepsilon^b/\rho_0} \rangle$ [Eq. (A3); dashed lines]. (c),(d) Cross-shelf profiles the mean wave heights (left y axis) and wavenumbers (right y axis). Left and right columns are with and without wave streaming. Asterisks mark the surf-zone edge. The four colors represent four types of incident waves. (e),(f) Wave rays for (e) SN waves and (f) SO waves both with streaming. The colors indicate wave heights.

vertical layers shows that 12 vertical layers are good enough to resolve the boundary layers and velocity profiles.

Initially the water is at rest with uniform density. Incident surface waves are prescribed the offshore (east) boundary, where the current velocity is nudged to the anti-Stokes drift. The north and south boundaries are periodic, and the west and east boundaries have zero net fluxes. The Coriolis parameter is $8.13 \times 10^{-5}\,\mathrm{s}^{-1}$ for a midlatitude.

The wave model is forced by the offshore boundary condition, which is the prescribed wave heights, periods, and directions of incident waves. The prescribed waves can be uniform or stochastic. Uniform waves have a constant height of 0.8 m and a constant period of 10 s; stochastic waves have the mean wave height and period same as the uniform waves, but the waves heights and periods have stochastic variations of 10% of the mean. Stochastic waves (Fig. 1b) are constructed with the solutions of a stochastic partial differential equation (appendix B). The total wave energy input at the offshore boundary is approximately equal between the stochastic and uniform waves. Here the stochastic waves represent a narrow period band around the wave-spectrum peak of the realistic waves recorded by a wave buoy (Figs. 1c,d). Although the stochastic waves are not full spectrum, they advance beyond uniform waves toward realistic ones. In addition, the wave incidence can be normal or oblique. The normal incidence is perpendicular to the shore, and the oblique incidence is at an angle of 30° (northwestward) relative to the shore normal. The stochastic waves also have a directional spread of 10° about their mean incidence. By combining uniform or stochastic waves with the normal or oblique incidence, we obtain four types of incident waves (UN, UO, SN, and SO; see Table 1). Then we conduct experiments for all wave types with and without wave streaming.

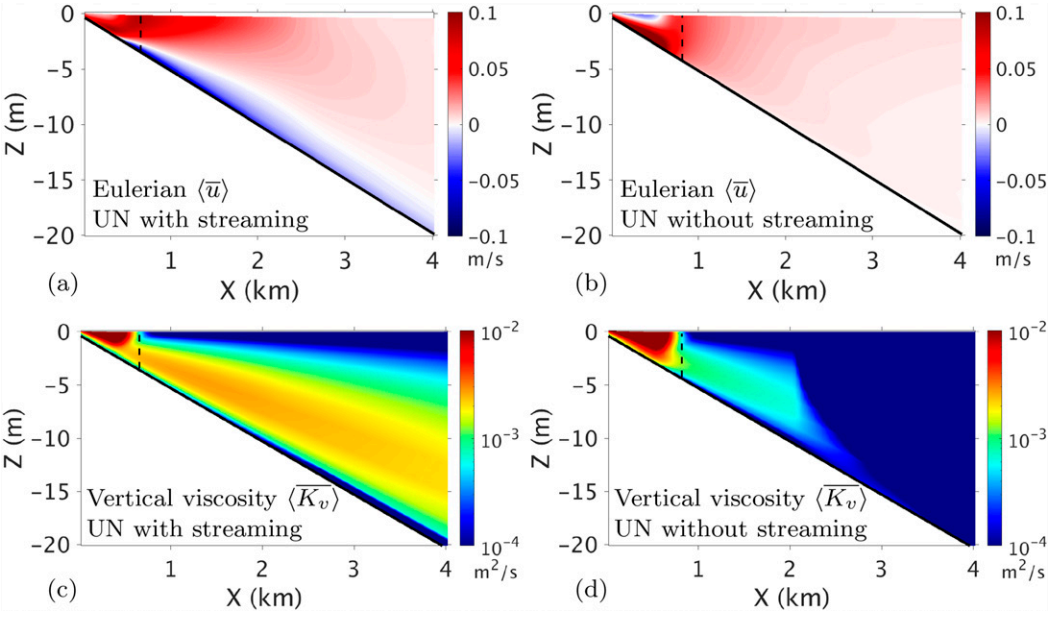

FIG. 3. (a),(b) Mean cross-shelf Eulerian current. (c),(d) Mean vertical eddy viscosity. Left and right columns are with and without wave streaming. Dashed lines delineate the surf-zone edge.

3. Results

a. Mean circulation

We define the "mean" as the average both over the alongshore direction and over the time period from day 5 to 10, when the mean circulation reaches a quasi-steady state. The mean quantity is denoted by $\langle\cdot\rangle$; the angle brackets $\langle\cdot\rangle$ denote the alongshore average, and the overline $\bar{\cdot}$ denotes the time average.

1) CROSS-SHELF CURRENTS

After the uniform or stochastic waves prescribed at the offshore boundary propagate into the model domain, they are

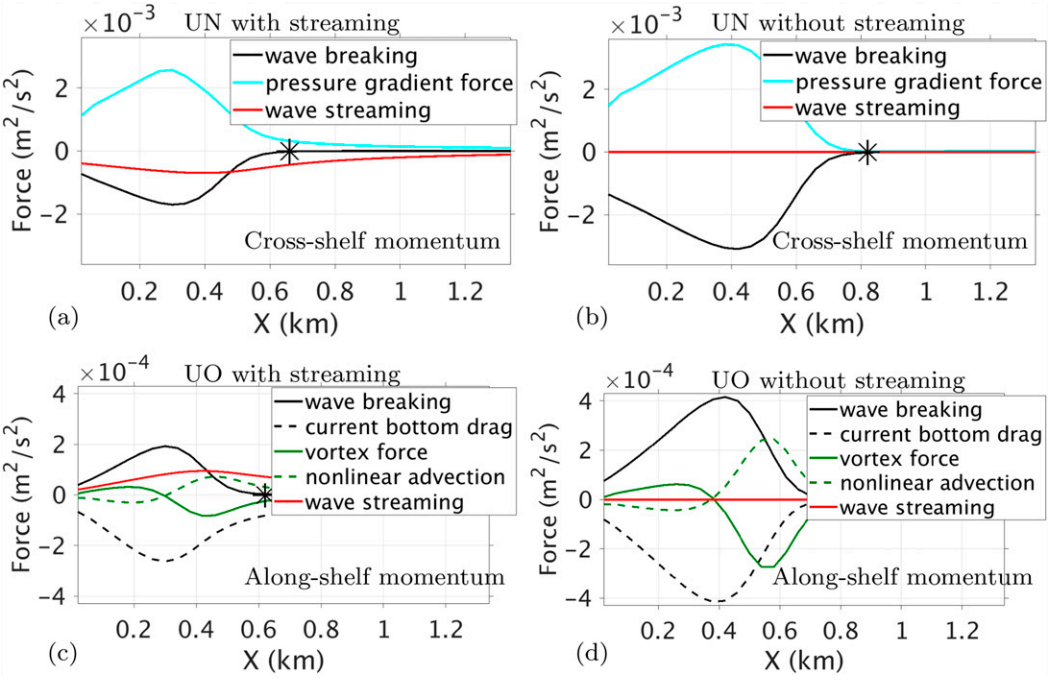

FIG. 4. Depth-integrated mean momentum balance per unit mass (a),(b) in the cross-shelf direction with UN waves and (c),(d) in the along-shelf direction with UO waves. Left and right columns are with and without wave streaming. Asterisks mark the surf-zone edge. Only important forces are displayed.

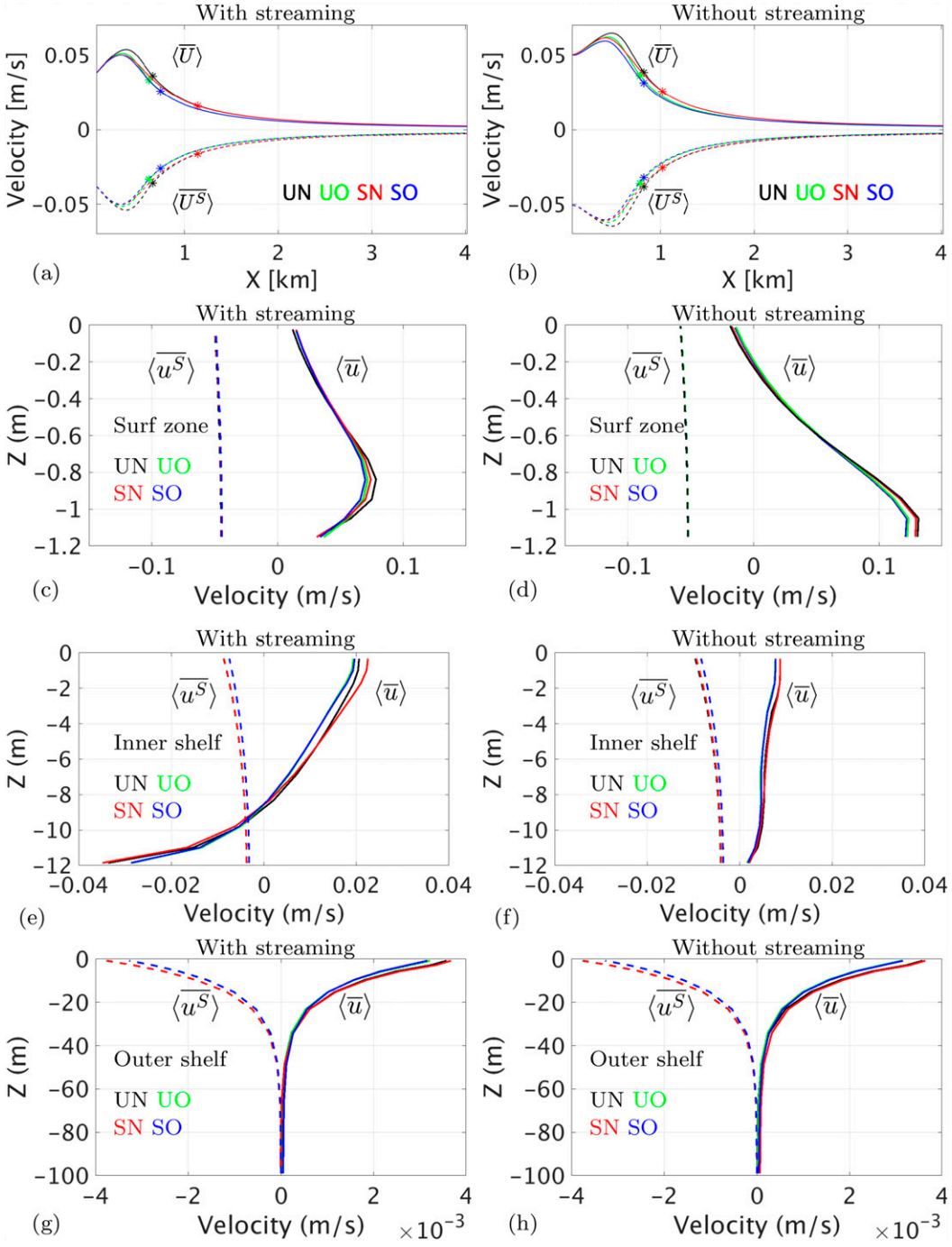

FIG. 5. (a),(b) Mean cross-shelf, depth-averaged Eulerian current and Stokes drift. Asterisks mark the surf-zone edge. Vertical profiles of the mean cross-shelf, depth-dependent Eulerian current and Stokes drift in the (c),(d) surf zone $x = 0.2$ km, (e),(f) inner shelf $x = 2.4$ km, and (g),(h) outer shelf $x = 20$ km. Left and right columns are with and without wave streaming. Solid and dashed lines denote the Eulerian current and Stokes drift.

governed by the wave model and obey the fundamental wave dynamics, including refraction, shoaling, bottom drag, and surface breaking (Fig. 2a). The shoaling increases the wavenumber and wave heights (Fig. 2c). Without bottom drag dissipation, the wave heights increase more via shoaling (Fig. 2d); besides, wave energy is dissipated by surface breaking only because of no bottom drag, resulting in larger breaking dissipation and a wider surf zone (Fig. 2b).

The stochastic waves spread directionally and therefore experience wave ray convergences during the propagation

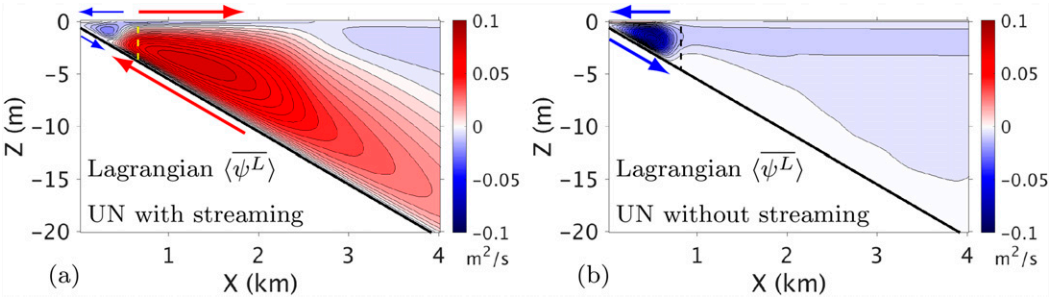

FIG. 6. Mean Lagrangian streamfunction $\langle\overline{\psi^L}\rangle$ defined in Eq. (2), (a) with and (b) without wave streaming. The surface and bottom arrows indicate the near-surface and near-bottom Lagrangian flow directions. Dashed lines delineate the surf-zone edge. Incident waves are UN, and other incident waves (UO, SN, SO) yield the $\langle\overline{\psi^L}\rangle$ similar to with and without wave streaming in (a) and (b), respectively.

(Figs. 2e,f). In the experiments with SN waves, the wave ray convergence is stronger, creating bigger waves (Fig. 2e). By contrast, SO wave rays take a longer path to the shore than SN wave rays due to the oblique incidence (Fig. 2f); thus, SO waves are dissipated more by bottom drag, lacking big waves as exist in SN waves. Because big waves break farther offshore, the surf zone with SN waves is wider (Figs. 2a,b).

Wave surface breaking induces a near-surface wave breaker force [Eq. (A4)] that can drive a near-surface onshore current in the surf zone. Meantime, the pressure gradient force generates a near-bottom offshore undertow to balance the onshore mass transport (Fig. 3b). Without wave streaming, the wave breaker force is balanced by the pressure gradient force in the cross-shelf direction (Fig. 4b) and by the current bottom drag in the along-shelf direction (Fig. 4d).

The wave streaming in the inner shelf manifests itself as a near-bottom onshore current (Fig. 3a), which meets the offshore undertow around the surf-zone edge, creating a near-bottom convergence zone. Also, the wave streaming force [Eq. (A6)] joins the momentum balance with breaker force (Figs. 4a,c).

The Stokes vortex force and Stokes–Coriolis force are insignificant in the surf zone with a normal wave incidence. Nonetheless, with an oblique incidence (Figs. 4c,d), the Stokes vortex force becomes significant and is balanced by the nonlinear advection (Newberger and Allen 2007; Uchiyama et al. 2009; Kumar et al. 2012).

Wave streaming enhances the vertical shear and near-bottom turbulence in the inner shelf; hence, the vertical eddy viscosity and bottom boundary layer thickness are increased (Fig. 3c). Without wave streaming, the vertical eddy viscosity

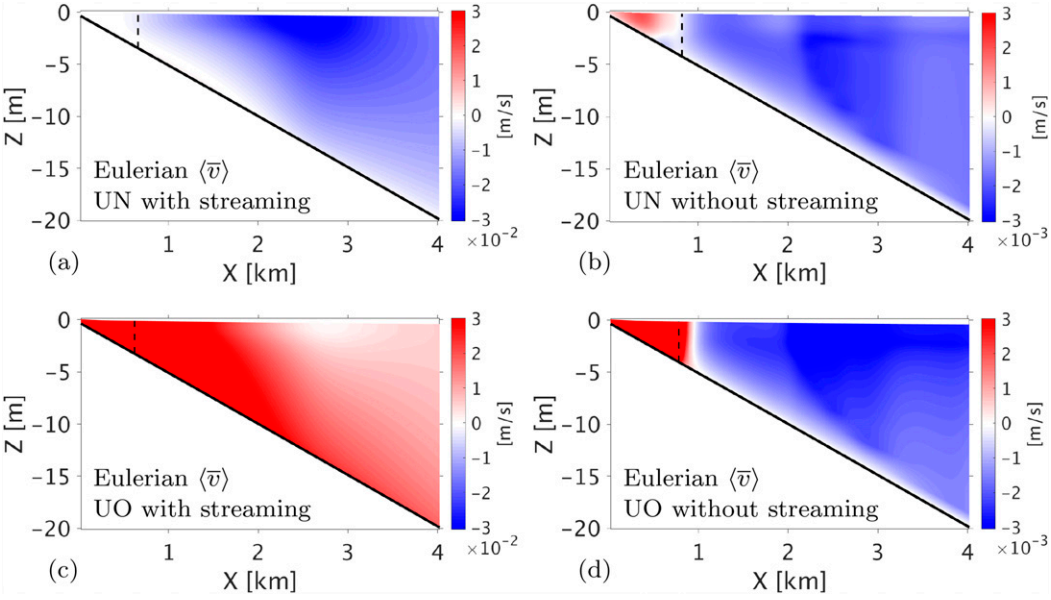

FIG. 7. Mean along-shelf Eulerian current with (a),(b) UN waves and (c),(d) UO waves. Left and right columns are with and without wave streaming. Dashed lines delineate the surf-zone edge.

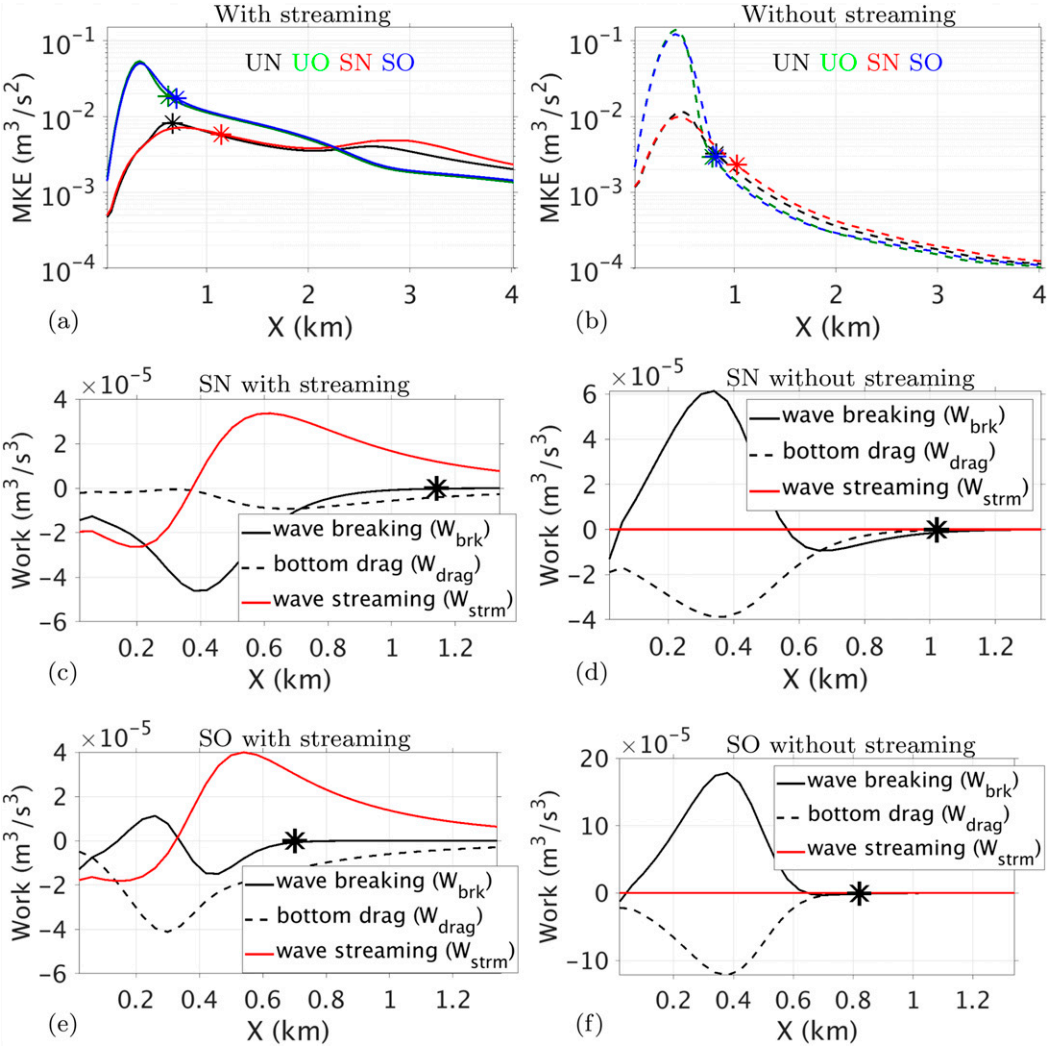

FIG. 8. Cross-shelf profiles of the depth-integrated (a),(b) MKE and (c)–(f) MKE budgets per unit mass with (c),(d) SN waves and (e),(f) SO waves. Left and right columns are with and without wave streaming. Asterisks mark the surf-zone edge. Only important work is displayed.

is weak in the inner shelf (Fig. 3d), and the inner-shelf bottom boundary layer is thin with a short offshore span. In addition, owing to the lack of surface forcing (e.g., wind stress and heat flux), the near-surface vertical mixing is weak in the inner shelf. In the surf zone, the vertical mixing is dominated by breaking waves (Battjes 1975), and the eddy viscosity without wave streaming is larger due to stronger wave breaking (Fig. 2b).

2) LAGRANGIAN OVERTURNING CIRCULATION

The Lagrangian velocity $\mathbf{u}^L$ is the sum of Eulerian velocity and Stokes drift (i.e., $\mathbf{u}^L = \mathbf{u} + \mathbf{u}^s$). For a steady flow, the continuity equation of the depth-averaged Lagrangian velocity $\mathbf{U}^L$ (Lentz and Fewings 2012) is

$$\frac{\partial(hU^L)}{\partial x} + \frac{\partial(hV^L)}{\partial y} \equiv \frac{\partial[h(U+U^s)]}{\partial x} + \frac{\partial[h(V+V^s)]}{\partial y} = 0. \quad (1)$$

Here h is the water depth, (U, V) is the depth-averaged Eulerian velocity, and (U^s, V^s) is the depth-averaged Stokes drift. When the flow is alongshore uniform (i.e., $\partial/\partial y = 0$) and has zero net flux across the shore boundary (i.e., $U^L|_{x=0} = 0$), Eq. (1) implies the depth-averaged $U^L(x) \equiv U + U^s = 0$ everywhere (Figs. 5a,b). However, the depth-dependent Lagrangian velocity $u^L(x, z) \equiv u + u^s$ is nonzero in the surf zone and inner shelf, viz., $u(x, z) \neq -u^s(x, z)$.

In the surf zone, the undertow $u(x, z)$ with and without wave streaming exhibits different profiles (Figs. 5c,d). In the inner shelf, the onshore wave streaming dominates the near-bottom current and decreases rapidly away from the bottom (Fig. 5e); without wave streaming, the inner-shelf current is nearly antiStokes (Fig. 5f). In the outer shelf, the current cancels the Stokes drift at each depth (Figs. 5g,h), leading to the Stokes–Coriolis balance. Due to the deep

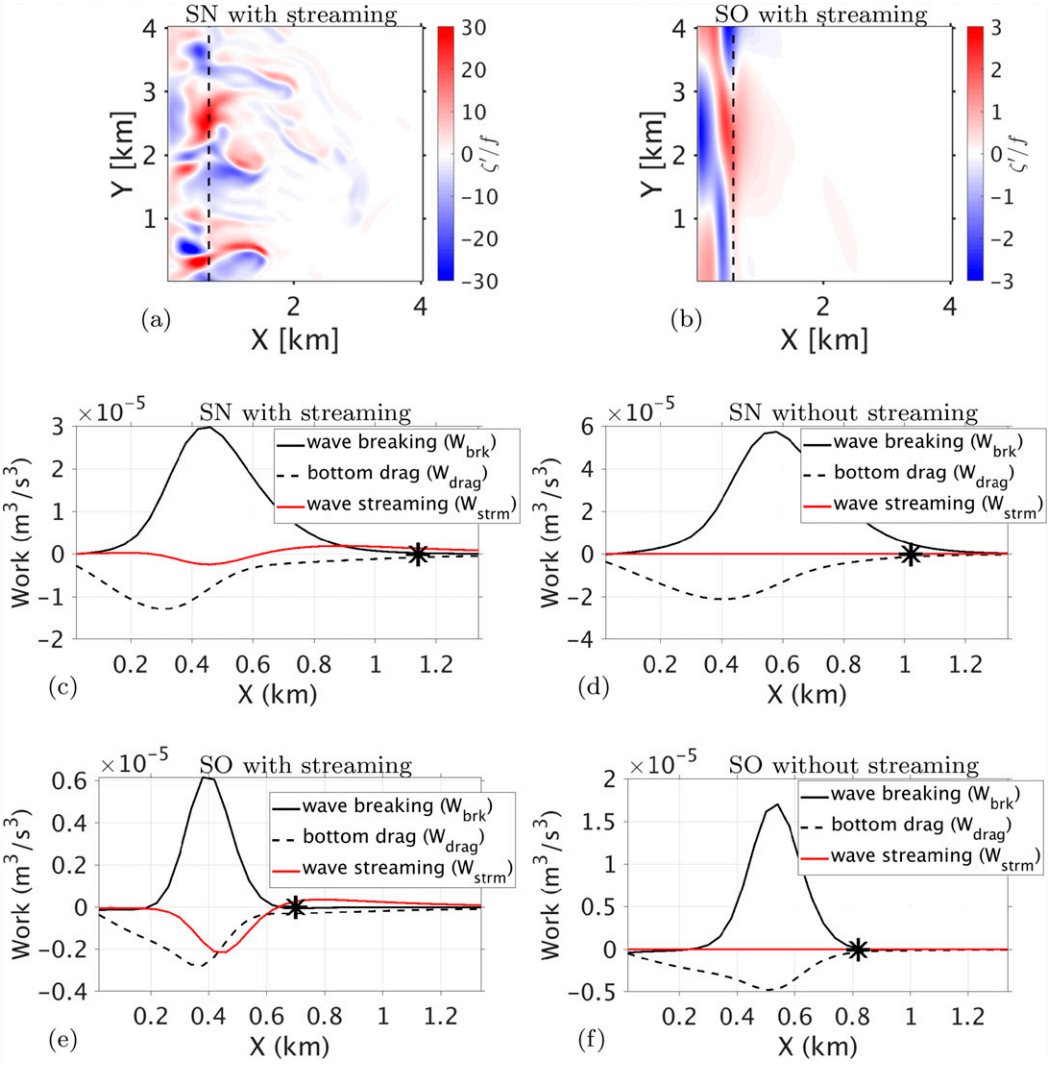

FIG. 9. (a),(b) Instantaneous surface vertical vorticity of surf eddies, normalized by the Coriolis parameter f, with (a) SN waves and (b) SO waves both with streaming. Dashed lines delineate the surf-zone edge. Cross-shelf profiles of the depth-integrated EKE budgets per unit mass with (c),(d) SN waves and (e),(f) SO waves. Left and right columns are with and without wave streaming. Asterisks mark the surf-zone edge. Only important work is displayed.

water there, the bottom drag dissipation and wave streaming are negligible.

To describe the Lagrangian overturning circulation in the depth- and cross-shelf section, we define a Lagrangian streamfunction $\psi^L(x, z)$ so that

$$u^L = -\frac{\partial \psi^L}{\partial z}, \quad w^L = \frac{\partial \psi^L}{\partial x}. \tag{2}$$

Without wave streaming (Fig. 6b), only one Lagrangian overturning circulation exists and occupies the entire surf zone. With wave streaming (Fig. 6a), the surf-zone Lagrangian overturning circulation gets smaller and weaker; meantime, an additional Lagrangian overturning circulation arises in the inner shelf and crosses the surf-zone edge.

3) ALONG-SHELF CURRENTS

With a normal wave incidence, there are no along-shelf components of the wave breaker force and streaming force. Nonetheless, the along-shelf Coriolis force fu^L associated with the Lagrangian velocity can drive an along-shelf current in the inner shelf (Figs. 7a,b), and the current is stronger with wave streaming due to stronger u^L.

With an oblique wave incidence, the along-shelf wave breaker force and streaming force arise. In the surf zone, the along-shelf breaker force drives an alongshore current (Figs. 7c,d), which is stronger without wave streaming. In the inner shelf, the along-shelf streaming force dominates over the Coriolis force and drives an along-shelf current (Fig. 7c), which is opposite to and stronger than that without wave streaming (Fig. 7d).

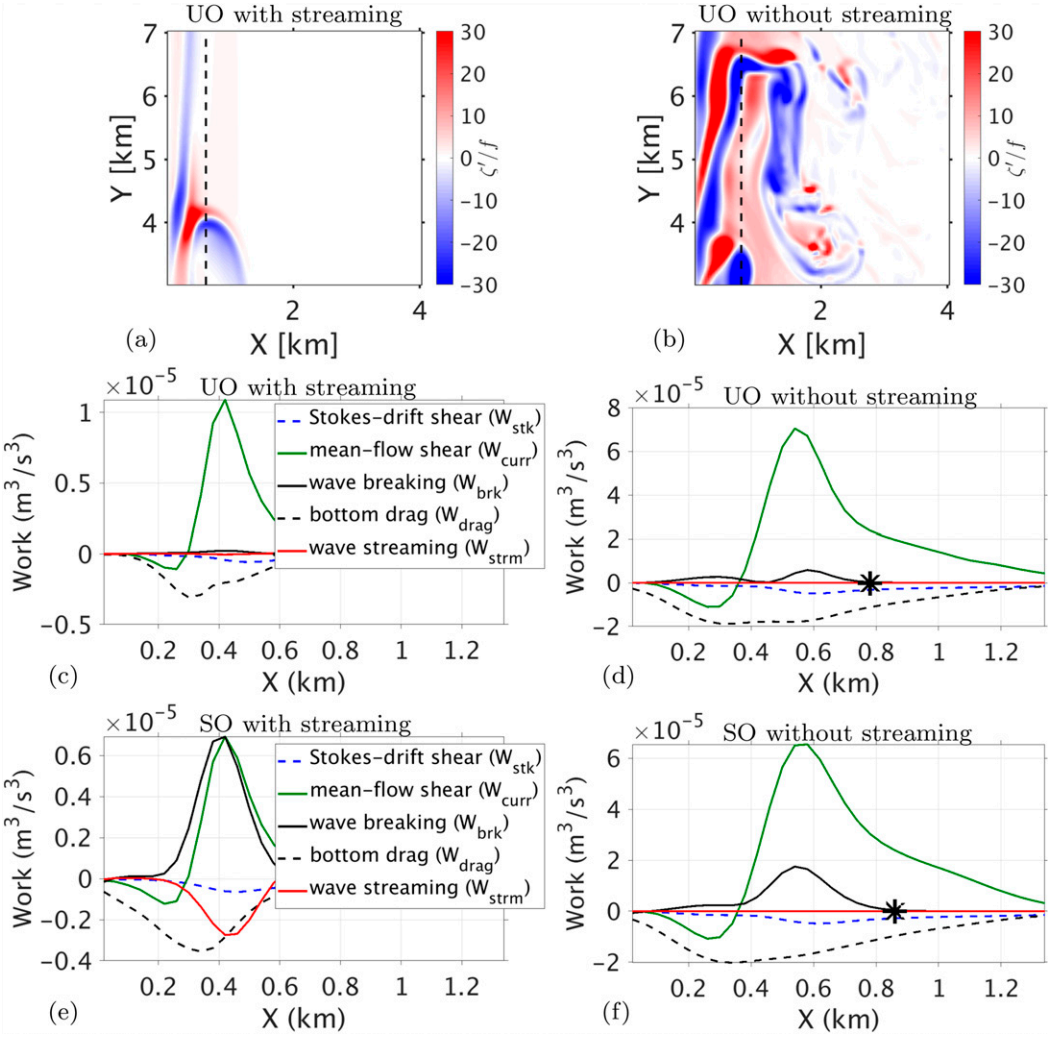

FIG. 10. (a),(b) Instantaneous surface vertical vorticity of surf eddies, normalized by the Coriolis parameter f, for UO waves (a) with and (b) without streaming. Dashed lines delineate the surf-zone edge. Cross-shelf profiles of the depth-integrated EKE budgets per unit mass with (c),(d) UO waves and (e),(f) SO waves. Left and right columns are with and without wave streaming. Asterisks mark the surf-zone edge. Only important work is displayed. All results are with reduced current bottom drag, in comparison to Fig. 9 with the default drag defined by Eq. (A7).

4) MEAN KINETIC ENERGY

The mean kinetic energy (MKE) is defined as $(1/2)(\langle\overline{u}\rangle^2 + \langle\overline{v}\rangle^2 + \langle\overline{w}\rangle^2)$, where $\langle\overline{u}\rangle$, $\langle\overline{v}\rangle$, $\langle\overline{w}\rangle$ denote the mean-flow components in the x, y, z directions. In terms of the MKE (Figs. 8a,b), the inner-shelf mean current is enhanced greatly by wave streaming, and the surf-zone mean current is increased significantly owing to the oblique wave incidence, which causes an alongshore current.

The budgets of depth-integrated MKE is summarized in Eq. (3):

$$\int dz \frac{d}{dt}(\mathrm{MKE}) = W_{\mathrm{brk}} + W_{\mathrm{strm}} + W_{\mathrm{drag}} + W_{\mathrm{StkCor}} + W_{\mathrm{Stk}} + W_{\mathrm{curr}} + W_{\mathrm{res}}. \quad (3)$$

The r.h.s. work is denoted by the symbols:

- $W_{\mathrm{brk}} = \int dz(\overline{F_i^b}\,\overline{u}_i)$ with the mean wave breaker force $\overline{F_i^b}$ (A4);
- $W_{\mathrm{strm}} = \int dz(\overline{F_i^f}\,\overline{u}_i)$ with the mean wave streaming force $\overline{F_i^f}$ (A6);
- $W_{\mathrm{drag}} = \overline{F^d}\,\overline{u}_i$ with the mean current bottom drag $\overline{F^d}$ (A7);
- $W_{\mathrm{StkCor}} = \int dz(-f\hat{k}\times\overline{u_j^s})\overline{u}_i$ with the mean Stokes–Coriolis force $(-f\hat{k}\times\overline{u_j^s})$;
- $W_{\mathrm{Stk}} = \int dz[-\overline{u}_i u_j(\partial u_j^s/\partial x_i)]$ with the mean Stokes shear force $[-u_j(\partial u_j^s/\partial x_i)]$;
- $W_{\mathrm{curr}} = \int dz[\overline{u_i' u_j'^{LT}}(\partial\overline{u}_i/\partial x_j)]$ with the mean-flow shear $\partial\overline{u}_i/\partial x_j$;
- W_{res} the residual including the transport divergence and the dissipation by viscosity.

The major work of interest is W_{brk} by the wave breaker force, W_{strm} by the wave streaming force, and W_{drag} by the wave-enhanced bottom drag. Without wave streaming (Figs. 8d,f), most MKE is produced by the wave breaker force and is dissipated

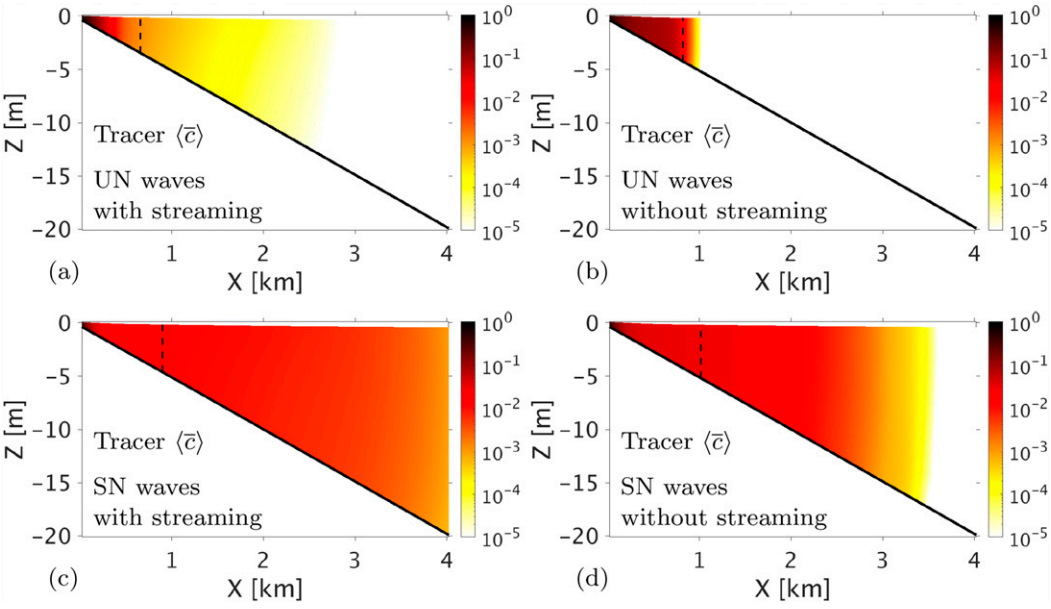

FIG. 11. Mean concentration (no units) of the shore-released passive tracers with (a),(b) UN waves and (c),(d) SN waves. Left and right columns are with and without wave streaming. Dashed lines delineate the surf-zone edge.

by the current bottom drag. With wave streaming (Figs. 8c,e), MKE is primarily produced by the wave streaming force, whereas the wave breaker force may even decrease the MKE, especially with a normal wave incidence (Fig. 8c).

b. *Surf eddies*

1) EDDIES BY BREAKING WAVES

Surf eddies originate in the surf zone but can reach beyond the surf-zone edge. A surf eddy may combine with its adjacent eddy of opposite vorticity to form a transient rip current (Peregrine 1998). Here surf eddies are revealed by the turbulent vertical vorticity calculated as $\zeta' = (\partial v'/\partial x) - (\partial u'/\partial y)$ (Figs. 9a,b), where (u', v') are the turbulent horizontal velocities.

SN waves induce alongshore-variable wave breaking that produces surf eddies and transient rip currents (Fig. 9a). By contrast, surf eddies with SO waves are much weaker and are mostly restricted within the surf zone without forming transient rip currents (Fig. 9b). Namely, an oblique wave incidence suppresses the surf eddies that are generated by the wave variation–induced, alongshore-variable wave breaking.

The budgets of depth-integrated eddy kinetic energy (EKE) is summarized in the Eq. (4):

$$\int dz \frac{d}{dt}(\mathrm{EKE}) = W'_{\mathrm{brk}} + W'_{\mathrm{strm}} + W'_{\mathrm{drag}} + W'_{\mathrm{StkCor}} + W'_{\mathrm{Stk}} + W'_{\mathrm{curr}} + W'_{\mathrm{res}}. \quad (4)$$

The r.h.s. work is denoted by the symbols:

- $W'_{\mathrm{brk}} = \int dz(F_i^{b'} u_i')$ with the turbulent wave breaker force $F_i^{b'}$ (A4);
- $W'_{\mathrm{strm}} = \int dz(F_i^{f'} u_i')$ with the turbulent wave streaming force $F_i^{f'}$ (A6);
- $W'_{\mathrm{drag}} = F^{d'} u_i'$ with the turbulent current bottom drag $F^{d'}$ (A7);
- $W'_{\mathrm{StkCor}} = \int dz(-f\hat{k} \times u_j^{s'}) u_i'$ with the turbulent Stokes–Coriolis force $(-f\hat{k} \times u_j^{s'})$;
- $W'_{\mathrm{Stk}} = \int dz\{-u_i'[u_j(\partial u_i^s/\partial x_i)]'\}$ with the turbulent Stokes shear force $\{-u_i'[u_j(\overline{\partial u_j^s/\partial x_i})]'\}$;
- $W'_{\mathrm{curr}} = \int dz[-u_i' u_j^{L'}(\partial \overline{u}_i/\partial x_j)]$ with the mean-flow shear $\partial \overline{u}_i/\partial x_j$;
- W'_{res} the residual including the transport divergence and the dissipation by viscosity.

In all cases, wave breaking produces nearly all the surf-zone EKE (W_{brk}, Figs. 9c–f). The EKE production with SO waves (Figs. 9e,f) is merely 20%–30% of that with SN waves (Figs. 9c,d), which explains the weak surf eddies with SO waves (Fig. 9b). Besides, wave streaming generally suppresses surf eddies (W_{strm}, Fig. 9e), and the EKE production with wave streaming (Figs. 9c,e) is only about half of that without wave streaming (Figs. 9d,f).

2) EDDIES BY SHEAR INSTABILITIES

Surf eddies can also be generated by the shear instability of surf-zone alongshore currents (Oltman-Shay et al. 1989; Özkan-Haller and Kirby 1999). When the current bottom drag is reduced [e.g., by decreasing the drag coefficient in Eq. (A7) to 0.0015], the shear instability may develop and evolve to surf eddies (Figs. 10a,b).

Surf eddies are stronger without wave streaming (Fig. 10b), because the shear production is stronger (W_{curr}, Fig. 10d). Particularly with uniform waves, the shear production contributes to nearly all the EKE (Figs. 10c,d). By wave–current interaction, surf eddies from the shear production introduce variations to uniform waves; thus, even if the offshore incident

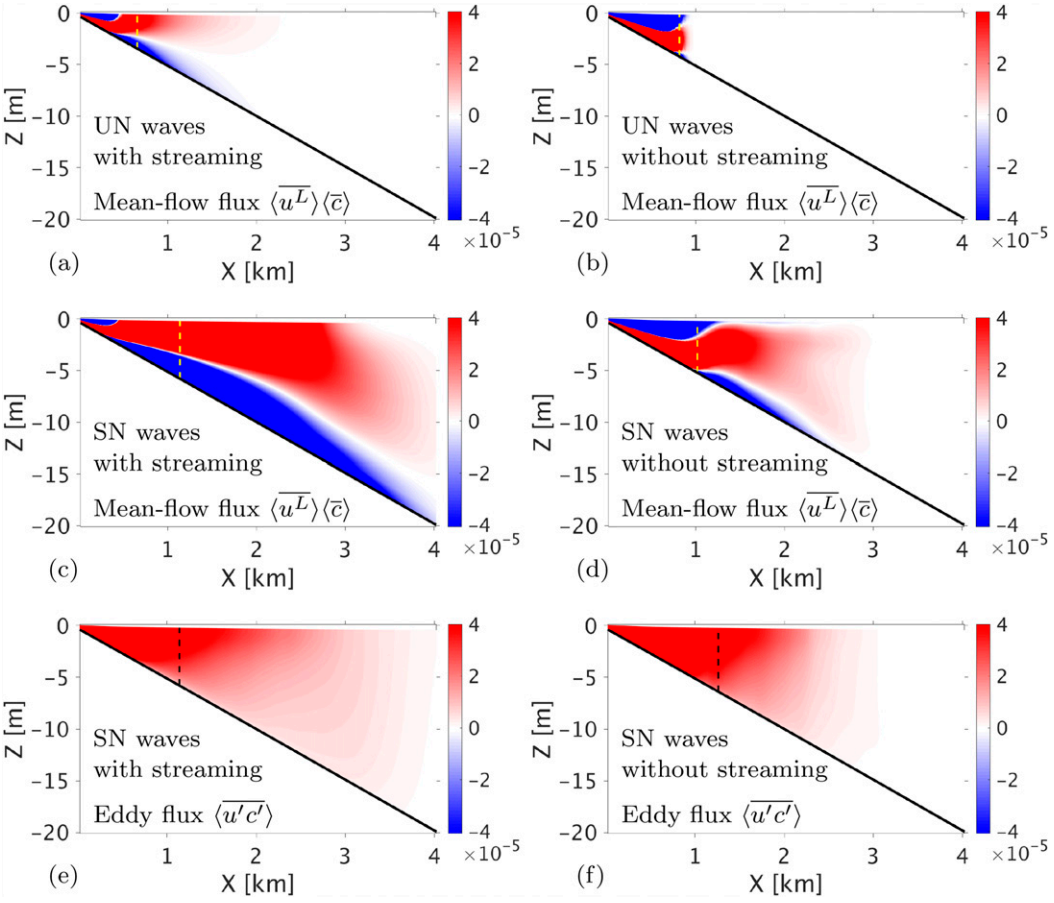

FIG. 12. Cross-shelf tracer fluxes by the (a)–(d) mean Lagrangian flow with UN waves in (a) and (b), and SN waves in (c) and (d); (e),(f) fluxes by the surf eddies with SN waves. Left and right columns are with and without wave streaming. Dashed lines delineate the surf-zone edge.

waves are uniform, alongshore-variable wave breaking may occur and produce EKE (W_{brk}, Fig. 10d).

For SO waves with streaming, the shear production and wave-breaking production are equally important (Fig. 10e), while the shear production prevails without wave streaming (Fig. 10f). Moreover, surf eddies are suppressed by the wave streaming (W_{strm}) and Stokes shear force (W_{stk}) (Figs. 10c–f).

c. *Cross-shelf transport*

Passive tracers are released at the shore continuously for the study of cross-shelf material transport. With uniform waves, surf eddies are absent and the tracers are transported by the mean Lagrangian flow only. Without wave streaming, the tracers are almost trapped within the surf zone and barely enters the inner shelf (Figs. 11b and 12b). With wave streaming, the inner-shelf Lagrangian overturning circulation forms and carries the tracers across the surf-zone edge into the inner shelf by the upper circulation segment (Figs. 11a and 12a); meantime, the lower circulation segment recycles the tracers from the inner shelf back to the surf zone (Fig. 12a).

With stochastic waves, surf eddies develop and carry the tracers across the surf-zone edge into the inner shelf (Figs. 12e,f); consequently, the inner-shelf tracer concentration is elevated remarkably (Figs. 11c,d). Particularly with wave streaming, the tracers are transported farther offshore by the inner-shelf Lagrangian overturning circulation (Figs. 11c and 12c).

4. Discussion

a. *Sensitivity to bottom roughness*

Wave streaming is parameterized with a streaming force given by Eqs. (A5) and (A6), in which the bottom roughness height z_o is crucial to determine the force magnitude. The default z_o in our experiments is 10^{-3} m, and here we explore how the different z_o changes the wave-driven circulation.

In general, the bottom drag dissipation (Fig. 13a) and the wave streaming (Fig. 13c) are elevated by increasing z_o. However, with a very large z_o up to 10^{-2} m, the maximum bottom drag dissipation is less than that with $z_o = 5 \times 10^{-3}$ m (Fig. 13a). Because the bottom drag dissipation is also proportional to the

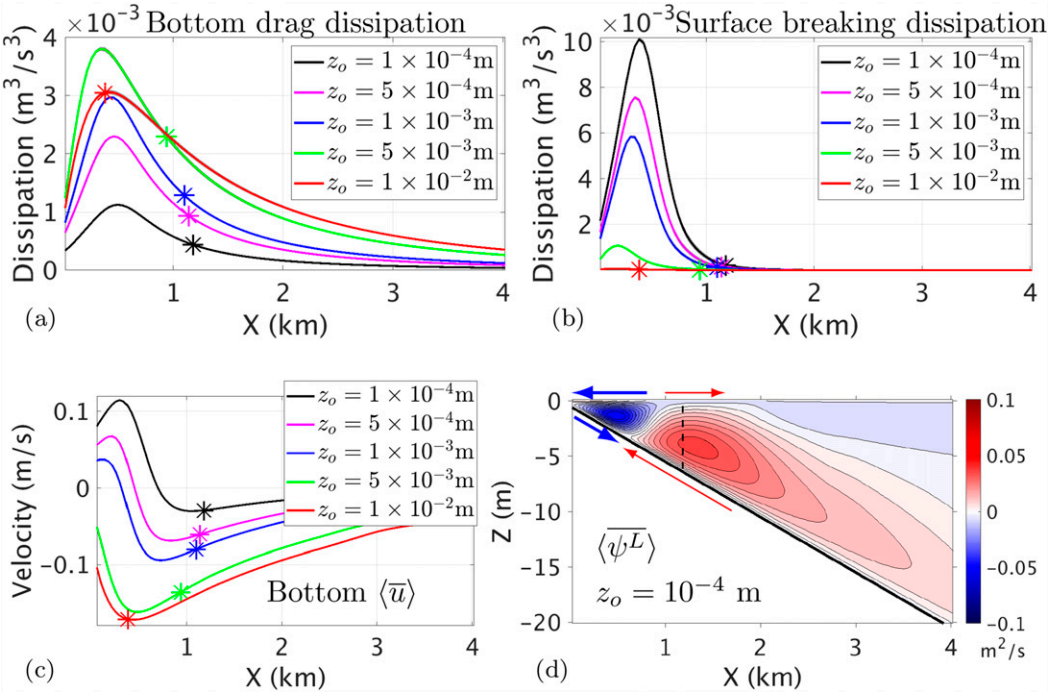

FIG. 13. Sensitivity to bottom roughness height z_o. Cross-shelf profiles of the mean wave dissipation (a) by the bottom drag $\langle \overline{\varepsilon^f/\rho_0} \rangle$ [Eq. (A5)] and (b) by the surface breaking $\langle \overline{\varepsilon^b/\rho_0} \rangle$ [Eq. (A3)]. (c) Mean cross-shelf bottom Eulerian current. (d) Mean Lagrangian streamfunction $\langle \overline{\psi^L} \rangle$ defined in Eq. (2) with $z_o = 10^{-4}$ m, in comparison to Fig. 6a with $z_o = 10^{-3}$ m. The asterisks in (a)–(c) and the dashed line in (d) mark the surf-zone edge. The 95% confidence intervals are shaded with gray. The incident waves are SN with streaming.

cubic wave height [Eq. (A5)], which is dampened greatly by a very large z_o.

The surface breaking dissipation decreases with increasing z_o (Fig. 13b), because with a larger z_o, more wave energy is dissipated by the bottom drag before breaking. Weak wave breaking leads to a weak breaker force [Eqs. (A3) and (A4)] and a small surf-zone undertow. Thus with increasing z_o, the onshore wave streaming is able to overwhelm the offshore undertow, turning the surf-zone, near-bottom current onshore (Fig. 13c).

Even with a very small $z_o = 10^{-4}$ m, the wave streaming can still induce an inner-shelf Lagrangian overturning circulation (Fig. 13d), though weaker than that with $z_o = 10^{-3}$ m (Fig. 6a). Besides, the wave breaking (Fig. 13b) and the surf-zone Lagrangian overturning circulation (Fig. 13d) are enhanced by decreasing z_o.

b. *Sensitivity to bottom slopes*

The default bottom slope in our experiments is 0.005, representing a gently sloping shelf; here we explore how the different slopes change the wave-driven circulation. When the bottom slope increases, the water depth at a fixed offshore location increases; accordingly, the location where surface waves start feeling the bottom moves shoreward, and so do the location where surface waves start breaking due to shallow depths (Fig. 14a). Namely, the offshore spans of the wave streaming (Fig. 14b) and the associated inner-shelf Lagrangian overturning circulation are shortened (Fig. 14c), and the surf zone narrows (Fig. 14a).

With a larger bottom slope, less wave energy is dissipated by the bottom drag before breaking (Fig. 14a); therefore, the wave heights remain bigger when waves start breaking, resulting in stronger breaking dissipation (Fig. 14a). Strong wave breaking enhances the offshore undertow and suppresses the onshore wave streaming (Fig. 14b).

Further, we design a more realistic bathymetry with a non-constant slope that decreases from 0.014 in the surf zone to 0.004 in the inner shelf (Fig. 14d). The surf-zone and inner-shelf Lagrangian overturning circulations form again (Fig. 14d) and resemble those in the bathymetry with a constant slope (Figs. 14c and 6a). So far we have explored various bottom slopes in the range of 0.004–0.02 that exist in the nature, and in such a wide range of bottom slopes, the wave streaming and its induced inner-shelf Lagrangian overturning circulation can survive.

c. *Sensitivity to wave variations*

The default wave variations in our experiments include a height variation $Q_{\mathrm{Hgt}} = 10\%$ of its mean, a period variation $Q_{\mathrm{Prd}} = 10\%$ of its mean, and a direction variation $Q_{\mathrm{Dir}} = 10°$ about its mean incident angle. Now we examine how the different Q_{Hgt}, Q_{Prd}, and Q_{Dir} change the wave-driven circulation, respectively; for example, when Q_{Dir} varies, both Q_{Hgt} and Q_{Prd} stay at zero.

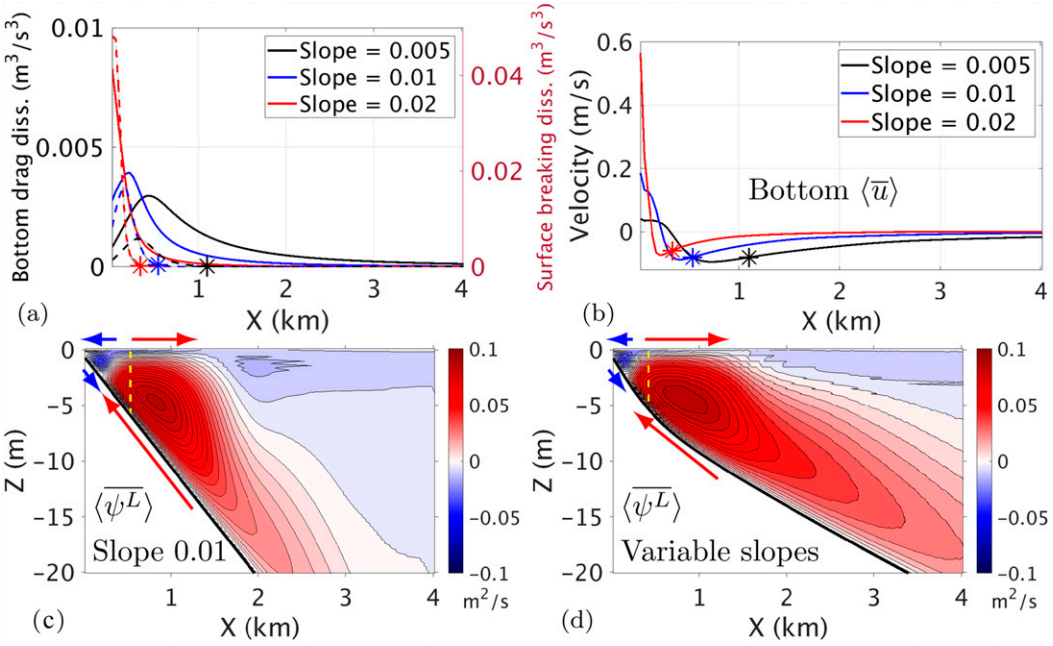

FIG. 14. Sensitivity to bottom slopes. (a) Cross-shelf profiles of the mean wave dissipation by the bottom drag $\langle\overline{\varepsilon^f/\rho_0}\rangle$ [Eq. (A5), solid lines and left y axis] and by the surface breaking $\langle\overline{\varepsilon^b/\rho_0}\rangle$ [Eq. (A3), dashed lines and right y axis]. (b) Mean cross-shelf bottom Eulerian current. (c),(d) Mean Lagrangian streamfunction $\langle\overline{\psi^L}\rangle$ defined in Eq. (2) with a constant slope of 0.01 in (c) and a nonconstant slope in (d), in comparison to Fig. 6a with a constant slope of 0.005. The slope in (d) decreases from 0.014 in the surf zone to 0.004 in the inner shelf. The asterisks in (a) and (b) and the dashed lines in (c) and (d) mark the surf-zone edge. The 95% confidence intervals are shaded with gray. The incident waves are SN with streaming.

The surf-zone EKE is elevated by increasing wave variations, and it is the largest with the wave direction variation Q_{Dir} (Fig. 15a); namely, directional-spread waves are inclined to induce strong surf eddies. Then we use the Q_{Dir} as a representative for wave variations.

As the Q_{Dir} increases, the mean wave breaking dissipation decreases (Fig. 15b), which then reduces the near-bottom undertow in the surf zone (Fig. 15c). In the inner shelf, however, the stronger surf eddies owing to a larger Q_{Dir} strengthen the eddy Reynolds stress, which enhances the near-surface mean flow (Fig. 15d).

5. Conclusions

Using numerical simulations in a nearshore region (surf zone and inner shelf), we examine how the wave streaming and wave variations affect the wave-driven circulation and the cross-shelf material transport. Also, sensitivities of the circulation to the bottom roughness, bottom slopes, wave variations are explored.

Wave streaming induces an inner-shelf Lagrangian overturning circulation, which facilitates the material exchange between the inner shelf and the surf zone by linking the two regions. Wave variations cause alongshore-variable wave breaking that generates surf eddies; nonetheless, such eddies can be suppressed by wave streaming or an oblique wave incidence. Moreover, surf eddies actively transport materials across the surf zone, beyond which the inner-shelf Lagrangian overturning circulation further spreads the material over the shelf.

Increasing the bottom roughness or decreasing the bottom slope can enhance wave streaming, and increasing wave variations can intensify surf eddies. Particularly, the directionally spread waves (direction variations) are effective to induce strong surf eddies.

Alongshore-variable bathymetry, such as rip channels, embayments, headlands, and submarine canyons, can impact the wave-driven circulation (Akan et al. 2020; MacMahan et al. 2006; Reniers et al. 2009; Dalrymple et al. 2011; Castelle et al. 2016), and it is worth exploring wave streaming in alongshore-variable bathymetry.

Density stratification can affect the nearshore wave-driven circulation (Kumar and Feddersen 2017b,c); in this study, however, stratification is not considered for simplification. In the companion study that includes stratification, Wang and McWilliams (2020, manuscript submitted to *Geophys. Res. Lett.*) discover an inner-shelf front induced by wave streaming.

The wave streaming in our experiments is parameterized by the Eqs. (A5) and (A6). The parameterization proposed by Xu and Bowen (1994) is also tried, and it gives similar but stronger wave streaming, possibly because the centimeter-thick wave bottom boundary layer is marginally resolved here. The requirement of vertical resolution for using the Xu–Bowen parameterization is discussed in appendix A [following Eq. (A6)]. Further, we suggest that more field measurements, particularly

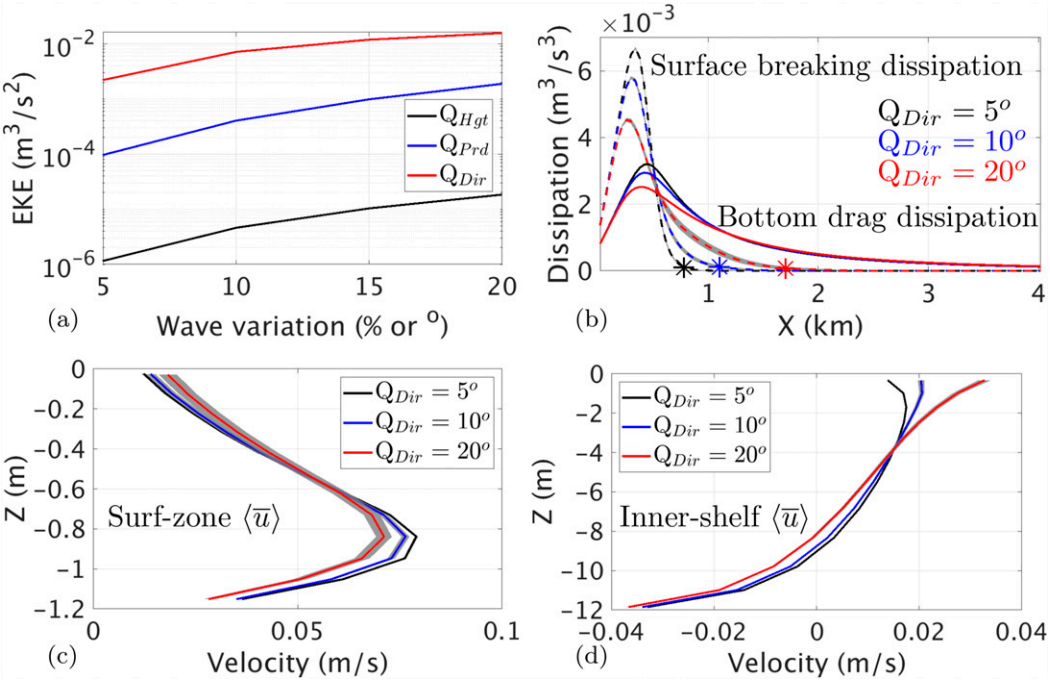

FIG. 15. Sensitivity to wave variations, including the wave height variation Q_{Hgt}, period variation Q_{Prd}, and direction variation Q_{Dir}. The Q_{Hgt} and Q_{Prd} are expressed in percent (%) of their mean, and the Q_{Dir} is expressed in angle degrees (°). (a) The depth-integrated EKE in the surf zone $x = 0.2$ km with different wave variations. (b) Cross-shelf profiles of the mean wave dissipation by the bottom drag $\langle \overline{\varepsilon^f/\rho_0} \rangle$ [Eq. (A5); solid lines] and by the surface breaking $\langle \overline{\varepsilon^b/\rho_0} \rangle$ [Eq. (A3); dashed lines]. Asterisks mark the surf-zone edge. (c),(d) Vertical profiles of the cross-shelf mean Eulerian current in the surf zone $x = 0.2$ km in (c) and the inner shelf $x = .2.4$ km in (d). The 95% confidence intervals are shaded with gray. The incident waves are SN with streaming.

in the inner shelf, are needed to assess the wave streaming, parameterizations, and the induced Lagrangian overturning circulation.

Acknowledgments. P.W. and J.M. appreciate the support by the Office of Naval Research (Grant N00014-15-1-2645) and by the National Science Foundation (Grant OCE-1355970). Y.U. is grateful for the support by the JSPS Grant-in-Aid for Scientific Research (Grant 15 KK0207, 17 K00653, 18H03798, and 19H00782) at Kobe University. The numerical simulations are done with the Extreme Science and Engineering Discovery Environment (XSEDE) supported by the National Science Foundation. Also, the authors sincerely thank the two reviewers for their constructive suggestions to improve this study.

APPENDIX A

Coupled Wave–Circulation Model

Equations of the momentum and passive tracers are (Uchiyama et al. 2010)

$$\begin{aligned}
\frac{\partial \mathbf{u}}{\partial t} + (\mathbf{u}\cdot\nabla_h)\mathbf{u} + w\frac{\partial \mathbf{u}}{\partial z} &= -f\hat{\mathbf{z}}\times\mathbf{u} - \nabla_h\phi + \frac{\partial}{\partial z}\left(K_v\frac{\partial \mathbf{u}}{\partial z}\right) - \nabla_h\mathscr{K} + \mathbf{J} + \boldsymbol{F}^w,\\
\frac{\partial \phi}{\partial z} + \frac{g\rho}{\rho_0} &= -\frac{\partial \mathscr{K}}{\partial z} + K,\\
\nabla_h\cdot\mathbf{u} + \frac{\partial w}{\partial z} &= 0,\\
\frac{\partial c}{\partial t} + (\mathbf{u}\cdot\nabla_h)c + w\frac{\partial c}{\partial z} + (\mathbf{u}^S\cdot\nabla_h)c + w^S\frac{\partial c}{\partial z} &= \frac{\partial}{\partial z}\left(K_t\frac{\partial c}{\partial z}\right) + \mathscr{S}.
\end{aligned} \tag{A1}$$

Here $(\mathbf{u}, w)$ is the 3D Eulerian velocity with $\mathbf{u} = (u, v)$, and $(\mathbf{u}^s, w^s)$ is the 3D Stokes drift, $\nabla_h = (\partial/\partial x, \partial/\partial y)$, f is the Coriolis parameter, and $\hat{\mathbf{z}}$ is a unit vertical vector. Also, ϕ is the dynamic pressure, and $\mathscr{K}$ is the Bernoulli head. The Stokes vortex force is $(\mathbf{J}, K)$, with the horizontal vector $\mathbf{J}$ incorporating the Stokes–Coriolis force. The variable $\boldsymbol{F}^w$ represents the nonconservative wave forces, ρ_0 is the mean density, and ρ is the density anomaly. The term c is the tracer concentration, and $\mathscr{S}$ is the tracer source; K_v (K_t) is the

vertical eddy viscosity (diffusivity), which includes the viscosity (diffusivity) induced by breaking waves (Battjes 1975).

The WKB wave model is (Uchiyama et al. 2010)

$$\frac{\partial \mathbf{k}}{\partial t} + [(\bar{\mathbf{u}} + \mathbf{c}_g)\cdot\nabla_h]\mathbf{k} = -\tilde{\mathbf{k}}\cdot\nabla_h\tilde{\bar{\mathbf{u}}} - \frac{\mathbf{k}\sigma}{\sinh 2kD}\nabla_h D,$$
$$\frac{\partial \mathscr{A}}{\partial t} + \nabla_h\cdot[(\bar{\mathbf{u}} + \mathbf{c}_g)\mathscr{A}] = -\frac{\varepsilon^w}{\sigma}. \quad \text{(A2)}$$

Here $\mathbf{k}$ is the horizontal wavenumber vector, $\mathbf{c}_g$ is the group velocity, and $\bar{\mathbf{u}}$ is the depth-averaged horizontal current velocity. The tilde symbol denotes the conjoined vector dot product. The term D is the water depth, σ is the intrinsic wave frequency, and $\mathscr{A}$ is the wave action. The term ε^w represents the wave dissipation, including the surface breaking and bottom drag.

The wave dissipation by surface breaking is determined by a quasi-empirical parameterization (Church and Thornton 1993),

$$\varepsilon^b = \frac{3\sqrt{\pi}}{16}\rho_0 g\frac{B_b^3\sigma}{2\pi D}H_{\text{rms}}^3\left\{1+\tanh\left[8\left(\frac{H_{\text{rms}}}{\gamma_b D}-1\right)\right]\right\} \times\left\{1-\left[1+\left(\frac{H_{\text{rms}}}{\gamma_b D}\right)^2\right]^{-5/2}\right\}, \quad \text{(A3)}$$

where H_{rms} is the RMS wave height and B_b and γ_b are empirical constants depending on wave breaking type and bathymetry. The wave breaker force is given by

$$\mathbf{F}^b = \frac{\varepsilon^b}{\sigma}\mathbf{k}. \quad \text{(A4)}$$

Optionally, the wave breaker force $\mathbf{F}^b$ can be distributed vertically with a prescribed shape function to represent shallow or deep breaking (Uchiyama et al. 2010).

The wave dissipation by bottom drag is determined by an empirical parameterization (Reniers et al. 2004a),

$$\varepsilon^f = \frac{1}{2\sqrt{\pi}}\rho_0 f_w|\mathbf{u}_{\text{orb}}^w|^3, \quad \text{(A5)}$$

where $|\mathbf{u}_{\text{orb}}^w| = \sigma H_{\text{rms}}/2\sinh(kD)$ is the near-bottom wave orbital velocity, $f_w = 1.39(\sigma z_o/|\mathbf{u}_{\text{orb}}^w|)^{0.52}$ is the wave friction factor (Soulsby 1997), and z_o is the bottom roughness height. The wave streaming force is given by

$$\mathbf{F}^f = \frac{\varepsilon^f}{\sigma}\mathbf{k}. \quad \text{(A6)}$$

The wave streaming parameterization with Eqs. (A5) and (A6) has been widely used in coastal studies (Uchiyama et al. 2010; Kumar et al. 2012; Marchesiello et al. 2015; Shanks et al. 2015; Morgan et al. 2017; Fujimura et al. 2018). Moreover, Xu and Bowen (1994) proposed a different parameterization for wave streaming [their Eq. (63)], which was used by Lentz et al. (2008) and Kumar et al. (2012) for inner-shelf studies. To apply the Xu–Bowen parameterization, a high vertical resolution of $\mathscr{O}(1)$ cm that is able to resolve the centimeter-thick wave bottom boundary layer is required (Lentz et al. 2008; Kumar et al. 2012). However, our simulations marginally resolve the wave bottom boundary layer, making the Xu–Bowen parameterization inappropriate here. Also, an unresolved wave bottom boundary layer may amplify the wave streaming and the associated shelf circulation. As noted by Kumar et al. (2012), the parameterization with Eqs. (A5) and (A6) is more suitable if the vertical resolution is not high enough to resolve the wave bottom boundary layer, while the Xu–Bowen parameterization is preferred with a high vertical resolution.

The current bottom drag is enhanced according to an empirical formula that combines the wave orbital velocity (Feddersen et al. 2000),

$$\mathbf{F}^d = 0.015\rho_0\left(\frac{k_a}{D}\right)^{1/3}\left[(1.16)^2+\left(\frac{|\mathbf{u}|}{|\mathbf{u}_{\text{rms}}^w|}\right)^2\right]^{1/2}|\mathbf{u}_{\text{rms}}^w|\mathbf{u}, \quad \text{(A7)}$$

where $\mathbf{u}_{\text{rms}}^w = \mathbf{u}_{\text{orb}}^w/\sqrt{2}$ is the near-bottom RMS wave orbital velocity, $k_a = 0.0125$ m is the apparent roughness (Ruessink et al. 2001).

APPENDIX B

Stochastic Waves

Stochastic waves are constructed with a space–time correlated stochastic process $F(y, t)$ that is a solution of a stochastic partial differential equation (Gillespie 1996),

$$dF(y,t) = \left[-\lambda F(y,t) + \gamma\frac{\partial^2 F}{\partial y^2}\right]dt + dW(y,t). \quad \text{(B1)}$$

Here λ and γ can be tuned to obtain a proper spatiotemporal correlation, which controls the spatial and temporal scales of surf eddies induced by stochastic waves; here the correlation is 10 wavelengths and 10 wave periods. The term $dW(y, t)$ denotes a "space–time" white noise process, roughly speaking, a Gaussian stochastic process with spatiotemporal correlations for $t_a, t_b \geq 0$, given by

$$\mathbb{E}[dW(y_a,t_a)dW(y_b,t_b)] = \delta(t_a - t_b)\delta(y_a - y_b). \quad \text{(B2)}$$

Equation (B1) is solved as follows: Over a grid of mesh size $dy = L_y/N_y$, the discrete approximation F_j^n of $F(jdy, ndt)$ is obtained via an explicit Euler–Maruyama scheme with a periodic boundary condition in y. The noise term $dW(y, t)$ is estimated by $\xi_j^n\sqrt{dt}$ at each time step ndt, and ξ_j^n is a N_y-dimensional vector of random variables each drawn independently from the standard normal distribution $\mathscr{N}(0, 1)$ with respect to $1 \leq j \leq N_y$ at each time step ndt.

REFERENCES

Akan, Ç., J. C. McWilliams, and Y. Uchiyama, 2020: Topographic and coastline influences on surf eddies. *Ocean Modell.*, **147**, 101565, https://doi.org/10.1016/j.ocemod.2019.101565.

Battjes, J., 1975: Modeling of turbulence in the surf zone. *Proc. Symp. Modeling Techniques*, San Francisco, CA, ASCE, 1050–1061.

——, 1988: Surf-zone dynamics. *Annu. Rev. Fluid Mech.*, **20**, 257–291, https://doi.org/10.1146/annurev.fl.20.010188.001353.

Bowen, A. J., 1969: Rip currents: 1. Theoretical investigations. *J. Geophys. Res.*, **74**, 5467–5478, https://doi.org/10.1029/JC074i023p05467.

Brink, K. H., 2016: Cross-shelf exchange. *Annu. Rev. Mar. Sci.*, **8**, 59–78, https://doi.org/10.1146/annurev-marine-010814-015717.

Brown, J. A., J. H. MacMahan, A. J. Reniers, and E. B. Thornton, 2015: Field observations of surf zone–inner shelf exchange

on a rip-channeled beach. *J. Phys. Oceanogr.*, **45**, 2339–2355, https://doi.org/10.1175/JPO-D-14-0118.1.

Castelle, B., T. Scott, R. Brander, and R. McCarroll, 2016: Rip current types, circulation and hazard. *Earth-Sci. Rev.*, **163**, 1–21, https://doi.org/10.1016/j.earscirev.2016.09.008.

Church, J. C., and E. B. Thornton, 1993: Effects of breaking wave induced turbulence within a longshore current model. *Coastal Eng.*, **20**, 1–28, https://doi.org/10.1016/0378-3839(93)90053-B.

Clark, D. B., S. Elgar, and B. Raubenheimer, 2012: Vorticity generation by short-crested wave breaking. *Geophys. Res. Lett.*, **39**, L24604, https://doi.org/10.1029/2012GL054034.

Craik, A. D., and S. Leibovich, 1976: A rational model for Langmuir circulations. *J. Fluid Mech.*, **73**, 401–426, https://doi.org/10.1017/S0022112076001420.

Dalrymple, R. A., J. H. MacMahan, A. J. Reniers, and V. Nelko, 2011: Rip currents. *Annu. Rev. Fluid Mech.*, **43**, 551–581, https://doi.org/10.1146/annurev-fluid-122109-160733.

Davies, A., and C. Villaret, 1999: Eulerian drift induced by progressive waves above rippled and very rough beds. *J. Geophys. Res.*, **104**, 1465–1488, https://doi.org/10.1029/1998JC900016.

Feddersen, F., 2014: The generation of surfzone eddies in a strong alongshore current. *J. Phys. Oceanogr.*, **44**, 600–617, https://doi.org/10.1175/JPO-D-13-051.1.

——, R. Guza, S. Elgar, and T. Herbers, 2000: Velocity moments in alongshore bottom stress parameterizations. *J. Geophys. Res.*, **105**, 8673–8686, https://doi.org/10.1029/2000JC900022.

Fujimura, A. G., A. J. Reniers, C. B. Paris, A. L. Shanks, J. H. MacMahan, and S. G. Morgan, 2018: Mechanisms of cross-shore transport and spatial variability of phytoplankton on a rip-channeled beach. *Front. Mar. Sci.*, **5**, 183, https://doi.org/10.3389/fmars.2018.00183.

Gillespie, D. T., 1996: The mathematics of Brownian motion and Johnson noise. *Amer. J. Phys.*, **64**, 225–240, https://doi.org/10.1119/1.18210.

Hally-Rosendahl, K., F. Feddersen, and R. Guza, 2014: Cross-shore tracer exchange between the surfzone and inner-shelf. *J. Geophys. Res. Oceans*, **119**, 4367–4388, https://doi.org/10.1002/2013JC009722.

Hasselmann, K., 1970: Wave-driven inertial oscillations. *Geophys. Astrophys. Fluid Dyn.*, **1**, 463–502, https://doi.org/10.1080/03091927009365783.

Henriquez, M., A. Reniers, B. Ruessink, and M. Stive, 2014: Piv measurements of the bottom boundary layer under nonlinear surface waves. *Coastal Eng.*, **94**, 33–46, https://doi.org/10.1016/j.coastaleng.2014.08.004.

Kranenburg, W. M., J. S. Ribberink, R. E. Uittenbogaard, and S. J. Hulscher, 2012: Net currents in the wave bottom boundary layer: On waveshape streaming and progressive wave streaming. *J. Geophys. Res.*, **117**, F03005, https://doi.org/10.1029/2011JF002070.

Kumar, N., and F. Feddersen, 2017a: The effect of Stokes drift and transient rip currents on the inner shelf. Part I: No stratification. *J. Phys. Oceanogr.*, **47**, 227–241, https://doi.org/10.1175/JPO-D-16-0076.1.

——, and ——, 2017b: The effect of Stokes drift and transient rip currents on the inner shelf. Part II: With stratification. *J. Phys. Oceanogr.*, **47**, 243–260, https://doi.org/10.1175/JPO-D-16-0077.1.

——, and ——, 2017c: A new offshore transport mechanism for shoreline-released tracer induced by transient rip currents and stratification. *Geophys. Res. Lett.*, **44**, 2843–2851, https://doi.org/10.1002/2017GL072611.

——, G. Voulgaris, J. C. Warner, and M. Olabarrieta, 2012: Implementation of the vortex force formalism in the coupled ocean-atmosphere-wave-sediment transport (coawst) modeling system for inner shelf and surf zone applications. *Ocean Modell.*, **47**, 65–95, https://doi.org/10.1016/j.ocemod.2012.01.003.

Lentz, S. J., 1995: U.S. contributions to the physical oceanography of continental shelves in the early 1990's. *Rev. Geophys.*, **33**, 1225–1236, https://doi.org/10.1029/95RG00177.

——, and M. R. Fewings, 2012: The wind-and wave-driven inner-shelf circulation. *Annu. Rev. Mar. Sci.*, **4**, 317–343, https://doi.org/10.1146/annurev-marine-120709-142745.

——, M. Fewings, P. Howd, J. Fredericks, and K. Hathaway, 2008: Observations and a model of undertow over the inner continental shelf. *J. Phys. Oceanogr.*, **38**, 2341–2357, https://doi.org/10.1175/2008JPO3986.1.

Long, J. W., and H. T. Özkan-Haller, 2009: Low-frequency characteristics of wave group–forced vortices. *J. Geophys. Res.*, **114**, C08004, https://doi.org/10.1029/2008JC004894.

Longuet-Higgins, M. S., 1953: Mass transport in water waves. *Philos. Trans. Roy. Soc. London*, **245A**, 535–581, https://doi.org/10.1098/rsta.1953.0006.

MacMahan, J. H., E. B. Thornton, and A. J. Reniers, 2006: Rip current review. *Coastal Eng.*, **53**, 191–208, https://doi.org/10.1016/j.coastaleng.2005.10.009.

——, A. J. Reniers, and E. B. Thornton, 2010: Vortical surf zone velocity fluctuations with 0 (10) min period. *J. Geophys. Res.*, **115**, C06007, https://doi.org/10.1029/2009JC005383.

Madsen, O. S., 1978: Mass transport in deep-water waves. *J. Phys. Oceanogr.*, **8**, 1009–1015, https://doi.org/10.1175/1520-0485(1978)008<1009:MTIDWW>2.0.CO;2.

Marchesiello, P., R. Benshila, R. Almar, Y. Uchiyama, J. C. McWilliams, and A. Shchepetkin, 2015: On tridimensional rip current modeling. *Ocean Modell.*, **96**, 36–48, https://doi.org/10.1016/j.ocemod.2015.07.003.

McWilliams, J. C., J. M. Restrepo, and E. M. Lane, 2004: An asymptotic theory for interaction of waves and currents in coastal waters. *J. Fluid Mech.*, **511**, 135–178, https://doi.org/10.1017/S0022112004009358.

Morgan, S. G., A. L. Shanks, J. MacMahan, A. J. Reniers, C. D. Griesemer, M. Jarvis, and A. G. Fujimura, 2017: Surf zones regulate larval supply and zooplankton subsidies to nearshore communities. *Limnol. Oceanogr.*, **62**, 2811–2828, https://doi.org/10.1002/lno.10609.

——, ——, J. H. MacMahan, A. J. Reniers, and F. Feddersen, 2018: Planktonic subsidies to surf-zone and intertidal communities. *Annu. Rev. Mar. Sci.*, **10**, 345–369, https://doi.org/10.1146/annurev-marine-010816-060514.

Newberger, P., and J. S. Allen, 2007: Forcing a three-dimensional, hydrostatic, primitive-equation model for application in the surf zone: 2. Application to duck94. *J. Geophys. Res.*, **112**, C08018, https://doi.org/10.1029/2006JC003474.

Nielsen, P., 2006: Sheet flow sediment transport under waves with acceleration skewness and boundary layer streaming. *Coastal Eng.*, **53**, 749–758, https://doi.org/10.1016/j.coastaleng.2006.03.006.

Nittrouer, C. A., and L. D. Wright, 1994: Transport of particles across continental shelves. *Rev. Geophys.*, **32**, 85–113, https://doi.org/10.1029/93RG02603.

Oltman-Shay, J., P. Howd, and W. Birkemeier, 1989: Shear instabilities of the mean longshore current: 2. Field observations. *J. Geophys. Res.*, **94**, 18 031–18 042, https://doi.org/10.1029/JC094iC12p18031.

Özkan-Haller, H. T., and J. T. Kirby, 1999: Nonlinear evolution of shear instabilities of the longshore current: A comparison of observations and computations. *J. Geophys. Res.*, **104**, 25 953–25 984, https://doi.org/10.1029/1999JC900104.

Peregrine, D., 1998: Surf zone currents. *Theor. Comput. Fluid Dyn.*, **10**, 295–309, https://doi.org/10.1007/s001620050065.

Pineda, J., 1994: Internal tidal bores in the nearshore: Warm-water fronts, seaward gravity currents and the onshore transport of neustonic larvae. *J. Mar. Res.*, **52**, 427–458, https://doi.org/10.1357/0022240943077046.

——, J. A. Hare, and S. Sponaugle, 2007: Larval transport and dispersal in the coastal ocean and consequences for population connectivity. *Oceanography*, **20**, 22–39, https://doi.org/10.5670/oceanog.2007.27.

Reniers, A. J. H. M., E. Thornton, T. Stanton, and J. Roelvink, 2004a: Vertical flow structure during sandy duck: Observations and modeling. *Coastal Eng.*, **51**, 237–260, https://doi.org/10.1016/j.coastaleng.2004.02.001.

——, J. Roelvink, and E. Thornton, 2004b: Morphodynamic modeling of an embayed beach under wave group forcing. *J. Geophys. Res.*, **109**, C01030, https://doi.org/10.1029/2002JC001586.

——, J. MacMahan, E. Thornton, T. Stanton, M. Henriquez, J. Brown, J. Brown, and E. Gallagher, 2009: Surf zone surface retention on a rip-channeled beach. *J. Geophys. Res.*, **114**, C10010, https://doi.org/10.1029/2008JC005153.

——, ——, F. J. Beron-Vera, and M. J. Olascoaga, 2010: Rip-current pulses tied to Lagrangian coherent structures. *Geophys. Res. Lett.*, **37**, L05605, https://doi.org/10.1029/2009GL041443.

——, E. Gallagher, J. MacMahan, J. Brown, A. Van Rooijen, J. Van Thiel de Vries, and B. Van Prooijen, 2013: Observations and modeling of steep-beach grain-size variability. *J. Geophys. Res. Oceans*, **118**, 577–591, https://doi.org/10.1029/2012JC008073.

Ruessink, B., J. Miles, F. Feddersen, R. Guza, and S. Elgar, 2001: Modeling the alongshore current on barred beaches. *J. Geophys. Res.*, **106**, 22 451–22 463, https://doi.org/10.1029/2000JC000766.

——, T. Van Den Berg, and L. Van Rijn, 2009: Modeling sediment transport beneath skewed asymmetric waves above a plane bed. *J. Geophys. Res.*, **114**, C11021, https://doi.org/10.1029/2009JC005416.

Ryan, J. P., and Coauthors, 2005: Coastal ocean physics and red tides: An example from Monterey Bay, California. *Oceanography*, **18**, 246–255, https://doi.org/10.5670/oceanog.2005.58.

Shanks, A. L., J. MacMahan, S. G. Morgan, A. J. M. Reniers, M. Jarvis, J. Brown, A. Fujimura, and C. Griesemer, 2015: Transport of larvae and detritus across the surf zone of a steep reflective pocket beach. *Mar. Ecol. Prog. Ser.*, **528**, 71–86, https://doi.org/10.3354/meps11223.

Sinnett, G., F. Feddersen, A. J. Lucas, G. Pawlak, and E. Terrill, 2018: Observations of nonlinear internal wave run-up to the surfzone. *J. Phys. Oceanogr.*, **48**, 531–554, https://doi.org/10.1175/JPO-D-17-0210.1.

Soulsby, R., 1997: *Dynamics of Marine Sands: A Manual for Practical Applications.* Thomas Telford, 249 pp.

Spydell, M. S., F. Feddersen, and S. Suanda, 2019: Inhomogeneous turbulent dispersion across the nearshore induced by surfzone eddies. *J. Phys. Oceanogr.*, **49**, 1015–1034, https://doi.org/10.1175/JPO-D-18-0102.1.

Suanda, S. H., and F. Feddersen, 2015: A self-similar scaling for cross-shelf exchange driven by transient rip currents. *Geophys. Res. Lett.*, **42**, 5427–5434, https://doi.org/10.1002/2015GL063944.

Trowbridge, J., and O. S. Madsen, 1984: Turbulent wave boundary layers: 2. Second-order theory and mass transport. *J. Geophys. Res.*, **89**, 7999–8007, https://doi.org/10.1029/JC089iC05p07999.

Trowbridge, J. H., and S. J. Lentz, 2018: The bottom boundary layer. *Annu. Rev. Mar. Sci.*, **10**, 397–420, https://doi.org/10.1146/annurev-marine-121916-063351.

Uchiyama, Y., J. C. McWilliams, and J. M. Restrepo, 2009: Wave-current interaction in nearshore shear instability analyzed with a vortex force formalism. *J. Geophys. Res.*, **114**, C06021, https://doi.org/10.1029/2008JC005135.

——, ——, and A. F. Shchepetkin, 2010: Wave–current interaction in an oceanic circulation model with a vortex-force formalism: Application to the surf zone. *Ocean Modell.*, **34**, 16–35, https://doi.org/10.1016/j.ocemod.2010.04.002.

van der A, D. A., T. O'Donoghue, A. G. Davies, and J. S. Ribberink, 2011: Experimental study of the turbulent boundary layer in acceleration-skewed oscillatory flow. *J. Fluid Mech.*, **684**, 251–283, https://doi.org/10.1017/jfm.2011.300.

Wang, P., and T. M. Özgökmen, 2018: Langmuir circulation with explicit surface waves from moving-mesh modeling. *Geophys. Res. Lett.*, **45**, 216–226, https://doi.org/10.1002/2017GL076009.

Weber, J. E. H., G. Broström, and Ø. Saetra, 2006: Eulerian versus Lagrangian approaches to the wave-induced transport in the upper ocean. *J. Phys. Oceanogr.*, **36**, 2106–2118, https://doi.org/10.1175/JPO2951.1.

Xu, Z., and A. Bowen, 1994: Wave-and wind-driven flow in water of finite depth. *J. Phys. Oceanogr.*, **24**, 1850–1866, https://doi.org/10.1175/1520-0485(1994)024<1850:WAWDFI>2.0.CO;2.